Rapid coastal deoxygenation due to ocean circulation shift in the NW Atlantic

Mariona Claret[1,2,3*], Eric D. Galbraith[4,5,3], Jaime B. Palter[6], Daniele Bianchi[7], Katja Fennel[8], Denis Gilbert[9], & John P. Dunne[10]

[1]*Joint Institute for the Study of the Atmosphere and the Ocean, Seattle, WA, USA.*

[2]*University of Washington, Seattle, WA, USA.*

[3]*Department of Earth and Planetary Sciences, McGill University, Montréal, QC, Canada*

[4]*Institució Catalana de Recerca i Estudis Avançats (ICREA), Barcelona, Spain.*

[5]*Institut de Ciència i Tecnologia Ambientals, Universitat Autònoma de Barcelona, Bellaterra, Barcelona, Spain.*

[6]*Graduate School of Oceanography, University of Rhode Island, Narragansett, RI, USA*

[7]*Department of Atmospheric and Oceanic Sciences, University of California, Los Angeles, CA, USA*

[8]*Department of Oceanography, Dalhousie University, Halifax, Nova Scotia, Canada*

[9]*Maurice Lamontagne Institute, Fisheries and Oceans Canada, Mont-Joli, QC, Canada*

[10]*NOAA Geophysical Fluid Dynamics Laboratory, Princeton, NJ, USA*

Global observations show that the ocean lost approximately 2% of its oxygen inventory over the last five decades [1–3], with important implications for marine ecosystems [4,5]. The rate of change varies with northwest Atlantic coastal waters showing a long-term drop [6,7] that vastly outpaces the global and North Atlantic basin mean deoxygenation rates [5,8]. However, past

work has been unable to resolve mechanisms of large-scale climate forcing from local processes. Here, we use hydrographic evidence to show a Labrador Current retreat is playing a key role in the deoxygenation on the northwest Atlantic shelf. A high-resolution global coupled climate-biogeochemistry model [9] reproduces the observed decline of saturation oxygen concentrations in the region, driven by a retreat of the equatorward-flowing Labrador Current and an associated shift toward more oxygen-poor subtropical waters on the shelf. The dynamical changes underlying the shift in shelf water properties are correlated with a slowdown in the simulated Atlantic Meridional Overturning Circulation [10]. Our results provide strong evidence that a major, centennial-scale change of the Labrador Current is underway, and highlight the potential for ocean dynamics to impact coastal deoxygenation over the coming century.

There is wide consensus that the global ocean oxygen (O_2) concentration is decreasing, and will continue to do so over the next century due to global warming [11,12]. Thus far, the O_2 inventory of the North Atlantic basin has not followed the general trend [2], but has instead shown marked spatial variability driven by natural climate oscillations [13,14] that approximately balance over the whole basin [15]. But despite the muted historical change for the North Atlantic on average, dramatic long-term deoxygenation trends have been reported over the last century on the northwest Atlantic shelf [6,7,16] (Fig. 1), a region that hosts a highly productive benthic ecosystem.

The recent deoxygenation trends have also been recorded in marine sediments in the region [17,18], where they stand out as unique occurrences over the last millennium, and paleoceanographic

records have documented warming, salinification and changing nutrient supply on the Scotian Shelf during the past century [19–21]. It has been speculated that these coastal changes reflect variations in the large-scale offshore circulation that involves the Gulf Stream, which transports oxygen-poor tropical and subtropical water masses northward, and the Labrador Current, which transports well-oxygenated water masses southward [7,20]. However, it has been difficult to piece together the observations given their sparsity, and both the ocean dynamics and biogeochemistry in this complex region are not well represented by the coarse resolution typical of global climate models [22–24], leaving the underlying mechanisms poorly understood.

Figure 2 shows updated historical time series for three well-studied sites on the Scotian Shelf and in the Gulf of Saint Lawrence that confirm the continued trajectories of previously-reported trends [6,7,16]. Although the observations show large decadal-scale variability, the long-term average rate of O_2 decline at Cabot Strait was $-0.51 \pm 0.24\ \mu\mathrm{M\,yr^{-1}}$ between 1960 and 2015 on isopycnal $\sigma_\theta = 27.25\,\mathrm{kg\,m^{-3}}$, while on the Central Scotian Shelf it was $-1.19 \pm 0.45\ \mu\mathrm{M\,yr^{-1}}$ between 1961 and 2014 at 150 m depth, more than twice as fast (Fig. S1). The O_2 trend at Cabot Strait is indistinguishable from the trend of $-0.5\,\mu$M yr^{-1} between 1958 and 2015 recently estimated from World Ocean Atlas data in waters of 100-400 m depth in the open ocean, south of the Scotian Shelf [3]. Oxygen concentrations can be conceptualized as the difference between a saturation concentration (O_2^{sat}) equal to the oxygen concentration the waters would have in equilibrium with the atmosphere given their temperature and salinity, and the Apparent Oxygen Utilization (AOU) due to the consumption of oxygen by heterotrophic organisms, such that $O_2 = O_2^{\mathrm{sat}} - \mathrm{AOU}$. The trends of O_2^{sat} are similar at the three sites (Fig. 2c, dots; Fig. S1) reflecting comparable trends of

temperature and salinity (Figs. 2a,b, dots; Fig. S2). This similarity implies that the main difference behind the large change on the Scotian Shelf, relative to the Cabot Strait, is due to differences in the AOU.

To characterize the dynamics behind this dramatic historical deoxygenation, we analyze a high-resolution global coupled climate model, forced by an idealized CO_2-driven global warming scenario (Methods). This model faithfully captures critical aspects of the northwest Atlantic circulation, specifically reducing a warm bias on the Scotian Shelf that is common to coarse resolution models in which the Gulf Stream extends too far north [23]. Moreover, it simulates a spatial pattern of surface cooling in the subpolar North Atlantic and warming on the Scotian Shelf that agrees well with historical observations; in the simulation, this pattern of sea surface temperature change is linked to a slowing of the Atlantic Meridional Overturning Circulation (AMOC) [10].

The model reproduces the general O_2^{sat} decline associated with increasing temperature and salinity at the three sites (Figs. 2a,b,c; solid lines). Thus, the model reveals a potential mechanism for the rapid deoxygenation observed on the Scotian Shelf: a change in the large-scale ocean circulation that shifts the balance of water masses in the region. However, the model does not reproduce the long-term decline of oxygen concentrations at the two sites where measurements are available. The constant total oxygen concentration simulated at these sites by the model reflects a compensation of the O_2^{sat} decline by a similar decrease in AOU. Thus, it would appear that the model captures the broad hydrographic change and O_2^{sat} decrease well, while simulating a process that slows oxygen utilization (thereby reducing AOU) that was not operating in nature during the

historical period.

The northwest Atlantic shelf is thought to be particularly sensitive to climate variability due to its position near the crossroads of the subtropical and subpolar circulation at the nearby the Grand Banks of Newfoundland (Fig. 1), an underwater plateau that forces the Labrador Current to take a sharp right hand turn in order to continue its trajectory as a western boundary current in contact with the shelf break. An association has been previously found between water column properties at the Tail of the Grand Banks (i.e. its southeastern tip, see Fig. 1), the position of the Gulf Stream, and the strength of the Atlantic Meridional Overturning Circulation (AMOC) in observations and models [10,23,25,26]: warmer temperatures at the Tail of the Grand Banks correspond to a more northward Gulf Stream trajectory and a weaker AMOC. Moreover, decadal variability in the Labrador Current transport around the Tail of the Grand Banks to the Scotian Shelf [27], including to the Laurentian Channel Mouth [28], has been found to influence the properties of slope waters (i.e. water masses at depths greater than 200 m and less than 3000 m, shaded white in Fig. 1). As half of the O_2 decline on the northwest Atlantic shelf has been shown to be due to a rising proportion of oxygen-poor subtropical waters [7], we hypothesize that the rapid 20th century O_2 decline was due to a retreat of the Labrador Current and the increasing presence of Gulf Stream waters at the Tail of the Grand Banks.

To test for this dynamical change, we calculated the historical depths of two subsurface isopycnals at the Tail of the Grand Banks from high-quality observations in the Hydrobase data repository (Methods). Both isopycnals shoal by more than 700 m from the subtropical side of

the Gulf Stream to the core of the Labrador Current (Fig. S3); thus, a reduced presence of the Labrador Current at the Tail of the Grand Banks would be expected to result in a deepening of these isopycnals over time. Indeed, the data show the isopycnal that enters the Laurentian Channel ($\sigma_\theta = 27.25\,\mathrm{kg\,m^{-3}}$) deepened at the Tail of the Grand Banks by $0.48 \pm 0.2\,\mathrm{m\,yr^{-1}}$ between 1920 and 2010 (Fig. 3a, dots), while an even faster deepening trend occurred on the denser isopycnal ($\sigma_1 = 32.2\,\mathrm{kg\,m^{-3}}$) with a rate of $1.30 \pm 0.36\,\mathrm{m\,yr^{-1}}$ over the same time period (Fig. 3b, dots). The simulated isopycnals in the same region also deepen as the model responds to the warming effect of an atmospheric CO_2 increase (Fig. 3, solid lines).

The deepening of isopycnals reflects a buoyancy gain by the upper water column, due to an increase in buoyant subtropical waters relative to dense subpolar waters, consistent with the modeled change in horizontal circulation (Fig. S4). Under doubled CO_2, the simulated Labrador Current weakens by as much as 8-10 Sv (1 Sv $\equiv 10^6\,\mathrm{m^3\,s^{-1}}$, see Methods for definition) north of the Grand Banks, as it approaches Orphan Knoll (Fig. S4). Associated with this reduced transport, the boundary between the cyclonic subpolar circulation and anticyclonic Gulf Stream migrates north, increasing the probability that the Gulf Stream and/or its associated eddies impinge on the Tail of the Grand Banks. The shift in Gulf Stream position and the Labrador Current slowdown is associated with a weakening of the AMOC [10,23], both of which may also be related to a weakening of the wind stress curl on the subpolar gyre simulated by the climate model (Fig. S5). An important association between the large-scale wind field and the northward excursions of the Gulf Stream is supported by recent findings that show that variability in northwest Atlantic shelf waters is correlated with interannual variability in the wind stress, with the mean position of the Gulf

Stream being closely tied to the mean zero wind stress curl line [28]. The consistency between the observations and the simulation strongly suggests that a climate-driven dynamical shift, toward enhanced impingement of the Gulf Stream on the Tail of the Grand Banks, is at least partly responsible for the shrinking influence of Labrador Current waters and the associated deoxygenation of the Scotian Shelf and Gulf of St. Lawrence.

Given that the simulated retreat of the Labrador Current and decrease of O_2^{sat} under warming appear to be consistent with the observed historical changes, we provide further analysis of the impacts on oxygen concentrations under continued warming as an indication of potential future trends (Figs. S1, S2; red lines). Focusing on an isopycnal surface, as the modeled Labrador Current continues to retreat, the supply of well-oxygenated waters rounding the Tail of the Grand Banks dwindles (supplemental video), and a large decrease of oxygen occurs throughout the coastal region, but with significant spatial variation (Fig. 4). The modeled O_2^{sat} concentrations decrease throughout the coastal region as the waters of a given density become warmer and saltier. This decrease is most pronounced where the isopycnal impinges on the continental shelf, and within the Laurentian Channel (Fig. 4b). The coastal O_2^{sat} decrease is amplified by increases of AOU to cause large O_2 decreases along the path of the Labrador Current and around the margin of the Grand Banks. However, it is opposed by AOU decreases (Fig. 4c) in the more southern coastal regions and Laurentian Channel, mitigating the simulated O_2 decrease (Fig. 4a).

Further mechanistic understanding of the simulated O_2^{sat} and AOU changes are provided by a water-mass mixing model on an isopycnal surface (Supplement). This approach shows that

the deoxygenation is primarily driven by a shift in ocean circulation, with additional contributions from warming and reduced ventilation of the Labrador Current end member. Taking the Laurentian Channel Mouth as a representative site, we find that the Labrador Current retreat drives about $2/3$ of the simulated oxygen loss (Tables S1–S3). The remaining changes are caused by changes in the Labrador Current end member properties resulting from a decrease in O_2^{sat} due to warming, and an increase in the end member AOU as intensified near-surface stratification impedes the formation of newly-ventilated waters (Fig. S6). A long-term trend toward reduced ventilation and retreat of Labrador Current waters is consistent with paleoceanographic reconstructions showing a slowdown of the AMOC and reduced ventilation in the Labrador Sea, where the Labrador Current is formed, prior to the 20th century [21]. As a result of these dynamical changes, the O_2^{sat} change is as much as $-32.8\,\mu$M in the northwest Atlantic slope and the Laurentian Channel (Fig. 4b, Table S2), whereas the average O_2^{sat} decline in the upper North Atlantic (above 300 m depth) in the *warming* simulation is only $-6.3\,\mu$M. In contrast, the simulated AOU decrease is in direct disagreement with historical records (Figs. 2, S1). This disagreement reflects a decrease in respiration rates along the pathway of circulation between the end members (Table S2), due to a reduction of simulated nutrient supply to the surface. The model inaccuracy likely arises from the relative simplicity of the biogeochemical model, which lacks many features such as anthropogenic nutrient inputs and interactions with the benthos. We therefore expect that future O_2 declines in this region may be significantly larger than simulated by the model, and could feasibly exceed the reduction in saturation.

The deoxygenation observed in the northwest Atlantic shelf is already altering the regional ecosystem [16,29] and, as shown by our results, is likely to become much more pronounced with con-

tinued global warming. These results emphasize the importance that open ocean dynamics can play in regional oxygen changes [5], explaining quasi-centennial O_2^{sat} trends of about $-0.21 \pm 0.03\,\mu$M yr^{-1} as observed between 1923 and 2017 in the Gulf of St. Lawrence (Fig. S1). This change in saturation concentration alone is more than double the total oxygen trend reported over the last 50 years in the upper layers of the North Atlantic, being $-0.075\,\mu$M yr^{-1} averaged above 1200 m [2] and about $-0.099\,\mu$M yr^{-1} for upper and intermediate waters [15]. Yet, given the pronounced decadal variability (Fig. 2), even the strong local trends in the Scotian Shelf would be undetectable without long observational time series. Moreover, because local circulation dynamics are difficult to resolve in global models, they may harbor surprises in other coastal regions. Finally, we speculate that the decline of oxygen concentrations on the northwest Atlantic shelf is a sensitive indicator of large-scale dynamical shifts offshore, which are potentially linked with a centennial-scale slowdown of the AMOC [10] and may ultimately influence the oxygen variability of the open North Atlantic [30].

1. Helm, K. P., Bindoff, N. L. & Church, J. A. Observed decreases in oxygen content of the global ocean. *Geophysical Research Letters* **38 (23)** (2011).

2. Schmidtko, S., Stramma, L. & Visbeck, M. Decline in global oceanic oxygen content during the past five decades. *Nature* **542**, 335–339 (2017).

3. Ito, T., Minobe, S., Long, M. C. & Deutsch, C. Upper ocean O_2 trends: 1958–2015. *Geophysical Research Letters* **44 (9)**, 4214–4223 (2017).

4. Breitburg, D. *et al.* Declining oxygen in the global ocean and coastal waters. *Science* **359**

(6371) (2018).

5. Levin, L. A. Manifestation, drivers, and emergence of open ocean deoxygenation. *Annual Review of Marine Science* **10 (1)**, 229–260 (2018).

6. Petrie, B. & Yeats, P. Annual and interannual variability of nutrients and their estimated fluxes in the Scotian Shelf - Gulf of Maine region. *Canadian Journal of Fisheries and Aquatic Sciences* **57 (12)**, 2536–2546 (2000).

7. Gilbert, D., Sundby, B., Gobeil, C., Mucci, A. & Tremblay, G.-H. A seventy-two-year record of diminishing deep-water oxygen in the St. Lawrence estuary: The northwest Atlantic connection. *Limnology and Oceanography* **50 (5)**, 1654–1666 (2005).

8. Gilbert, D., Rabalais, N. N., Díaz, R. J. & Zhang, J. Evidence for greater oxygen decline rates in the coastal ocean than in the open ocean. *Biogeosciences* **7 (7)**, 2283–2296 (2010).

9. Dufour, C. O. *et al.* Role of mesoscale eddies in cross-frontal transport of heat and biogeochemical tracers in the Southern Ocean. *Journal of Physical Oceanography* **45 (12)**, 3057–3081 (2015).

10. Caesar, L., Rahmstorf, S., Robinson, A., Feulner, G. & Saba, V. Observed fingerprint of a weakening Atlantic Ocean overturning circulation. *Nature* **556**, 191–196 (2018).

11. Keeling, R. F., Körtzinger, A. & Gruber, N. Ocean deoxygenation in a warming world. *Annual Review of Marine Science* **2 (1)**, 199–229 (2010).

12. Long, M. C., Deutsch, C. & Ito, T. Finding forced trends in oceanic oxygen. *Global Biogeochemical Cycles* **30 (2)**, 381–397 (2016).

13. Johnson, G. C. & Gruber, N. Decadal water mass variations along 20°W in the Northeastern Atlantic Ocean. *Progress in Oceanography* **73 (3)**, 277–295 (2007).

14. Frölicher, T. L., Joos, F., Plattner, G.-K., Steinacher, M. & Doney, S. C. Natural variability and anthropogenic trends in oceanic oxygen in a coupled carbon cycle-climate model ensemble. *Global Biogeochemical Cycles* **23 (1)** (2009).

15. Stendardo, I. & Gruber, N. Oxygen trends over five decades in the North Atlantic. *Journal of Geophysical Research: Oceans* **117 (C11)** (2012).

16. Brennan, C. E., Blanchard, H. & Fennel, K. Putting temperature and oxygen thresholds of marine animals in context of environmental change: A regional perspective for the Scotian Shelf and Gulf of St. Lawrence. *PLOS ONE* **11 (12)**, 1–27 (2016).

17. Thibodeau, B., de Vernal, A., Hillaire-Marcel, C. & Mucci, A. Twentieth century warming in deep waters of the Gulf of St. Lawrence: A unique feature of the last millennium. *Geophysical Research Letters* **37**, L17604 (2010).

18. Genovesi, L. *et al.* Recent changes in bottom water oxygenation and temperature in the Gulf of St. Lawrence: Micropaleontological and geochemical evidence. *Limnology and Oceanography* **56 (4)**, 1319–1329 (2011).

19. Keigwin, L., Sachs, J. & Rosenthal, Y. A 1600-year history of the Labrador Current off Nova Scotia. *Climate Dynamics* **12**, 53–62 (2003).

20. Sherwood, O. A., Lehmann, M. F., Schubert, C. J., Scott, D. B. & McCarthy, M. D. Nutrient regime shift in the western North Atlantic indicated by compound-specific δ15N of deep-sea gorgonian corals. *Proceedings of the National Academy of Sciences of the United States of America* **108 (3)**, 1011–1015 (2011).

21. Thornalley, D. J. R. *et al.* Anomalously weak Labrador Sea convection and Atlantic overturning during the past 150 years. *Nature* **556**, 227–230 (2018).

22. Loder, J. W., van der Baaren, A. & Yashayaev, I. Climate comparisons and change projections for the Northwest Atlantic from six CMIP5 models. *Atmosphere-Ocean* **53 (5)**, 529–555 (2015).

23. Saba, V. S. *et al.* Enhanced warming of the Northwest Atlantic Ocean under climate change. *Journal of Geophysical Research: Oceans* **121 (1)**, 118–132 (2016).

24. Lavoie, D., Lambert, N. & Gilbert, D. Projections of future trends in biogeochemical conditions in the northwest Atlantic using CMIP5 Earth system models. *Atmosphere-Ocean* **0**, 1–23 (2017).

25. Joyce, T. M. & Zhang, R. On the path of the Gulf Stream and the Atlantic Meridional Overturning Circulation. *Journal of Climate* **23 (11)**, 3146–3154 (2010).

26. Buckley, M. W. & Marshall, J. Observations, inferences, and mechanisms of the Atlantic Meridional Overturning Circulation: A review. *Reviews of Geophysics* **54 (1)**, 5–63 (2016).

27. Petrie, B. & Drinkwater, K. Temperature and salinity variability on the Scotian Shelf and in the Gulf of Maine 1945-1990. *Journal of Geophysical Research: Oceans* **98 (C11)**, 20079–20089 (1993).

28. Peterson, I., Greenan, B., Gilbert, D. & Hebert, D. Variability and wind forcing of ocean temperature and thermal fronts in the Slope Water region of the Northwest Atlantic. *Journal of Geophysical Research: Oceans* **122 (9)**, 7325–7343 (2017).

29. Bianucci, L., Fennel, K., Chabot, D., Shackell, N. & Lavoie, D. Ocean biogeochemical models as management tools: a case study for Atlantic wolffish and declining oxygen. *ICES Journal of Marine Science* **73 (2)**, 263–274 (2016).

30. Tagklis, F., Bracco, A. & Ito, T. Physically driven patchy O_2 changes in the North Atlantic Ocean simulated by the CMIP5 Earth system models. *Global Biogeochemical Cycles* **31**, 1218–1235 (2017).

Acknowledgements The authors thank Andrew Cogswell & Roger Pettipas from Fisheries and Oceans Canada for providing hydrographic data in the Central Scotian Shelf, and Catherine E. Brennan for providing the data for the oxygen time series in the Central Scotian Shelf. The authors also acknowledge many scientist at NOAA GFDL that configured and ran the climate model, without whose efforts this work would not have been possible. This project has received funding from the European Research Council (ERC) under the European Unions Horizon 2020 research and innovation programme (grant agreement No 682602). EDG acknowledges financial support from the Spanish Ministry of Economy and Competitiveness, through the Mara de Maeztu Programme for Centres/Units of Excellence (MDM-2015-0552). The Canadian Foundation

for Innovation provided the computing resources for model analysis. DB acknowledges support from NOAA grant NA15NOS4780186.

Author contributions E.D.G., J.B.P., and D.B. conceived the study. M.C., D.G., and K.F. assembled and analyzed observational data. M.C. and D.B performed model output analyses. J.P.D. participated in the design of the CM2.6-miniBLING experiments. M.C, E.D.G, J.B.P., and D.B. wrote a first draft of the manuscript. All authors discussed the results and provided input to the manuscript.

Competing Interests The authors declare no competing financial interests.

Correspondence Requests for materials should be addressed to M.C. or E.D.G.

Methods

Observational data. Instrument accuracy and analyses. Hydrographic data for Cabot Strait and the Laurentian Channel Mouth has been compiled, maintained, and quality-controlled by the Bedford Institute of Oceanography (BIO). Temperature data was sampled before 1943 using reversing thermometers mounted on bottles (accuracy ± 0.01°C), after 1943 using mechanical bathythermographs (accuracy ± 0.1°C), and from 1969 onward a variety of Conductivity-Temperature-Depth (CTD) models have been used with accuracy of ± 0.01°C or better [7]. Salinity data before 1969 was sampled from bottles (accuracy ± 0.05) and after 1969 using CTDs (accuracy of ± 0.01 or higher) [7]. Oxygen data has been developed, maintained, and quality-controlled by Fisheries Ocean Canada (DFO). This oxygen data was measured using Winkler tritations with an accuracy of ± 0.3-5 μM [7]. Time series are constructed by spatially averaging data interpolated on isopycnal

$\sigma_\theta = 27.25\,\mathrm{kg\,m^{-3}}$ over areas delimited by four coordinate pairs (Fig. 1). For Cabot Strait those are (60.74°W, 47.26°N), (59.43°W, 48.03°N), (58.70°W, 47.50°N), and (60.22°W, 46.52°N); while for the Laurentian Channel Mouth they are (57.83°W, 45.20°N), (57.24°W, 44.42°N), (55.86°W, 44.88°N); and (56.46°W, 45.67°N).

At the central Scotian Shelf, hydrographic data has been quality-controlled by DFO. Before late 1960s, temperature and salinity data was sampled using bottles with typical accuracies of ± 0.01°C and ± 0.01-0.03‰ [31], respectively. In the mid to late 1960s, hydrographic measurements were made with a early CTD that had an accuracy of ± 0.01°C for temperature and ± 0.01 for salinity; which improved to ± 0.001°C for temperature and ± 0.003 for salinity with the introduction of modern CTDs in the late 1980s (Brian Petrie, pers. comm. 2018). Oxygen data has been compiled and quality-controlled by Catherine E. Brennan. Oxygen data between 1961 and 1999 was measured using Winkler tritation (standard accuracy for this method performed on ships using bottle samples is ± 0.9-$1.8\,\mu$M [31]) and between January 2012 and December 2014 using Aanderaa optodes mounted on benthic pods (accuracy of $\pm 8\,\mu$M with two-point calibration; Catherine E. Brennan, pers. comm. 2018). Hydrographic time series correspond to data averaged over a box that extends zonally from 62°W to 64°W, meridionally from 43°N to 45°N, and vertically from 145 m to 155 m. The oxygen time series between 1961 and 1999 at 150 m depth is based on reported oxygen anomaly time series [6] plus a mean value of $179.7\,\mu$M computed from a subset of the original dataset [16] as the complete dataset is unavailable. For the period from November 2012 to April 2014, oxygen data in this region is interpolated at 150 m from high-resolution observations of two benthic pods [16], one at 133 m depth (63.10°W, 44.09°N) and the other one at 160 m (63.19°W,

43.91°N).

Historical time series of the depth of two isopycnals at the Tail of the Grand Banks (TGB) are computed using data extracted from HydroBase3, which is a global database of observed profiles that is quality-controlled, compiled, and made available by the Woods Hole Oceanographic Institution (WHOI). The data was extracted for the time period between 1920 and 2012, and the region that extends zonally from 53°W to 47.5°W and meridionally from 41.5°N to 44°N (see Fig. 1). Only data flagged as *good measurement* are considered. The resulting subdata comprises vertical profiles from bottles (86%), CTD casts (9%), and Argo floats (5%). Historical hydrographic data was sampled using bottles until the 1980s with an accuracy of ±0.01-0.02°C for temperature and ±0.01-0.03‰ for salinity as reported for measurements carried at WHOI [31]. CTDs were introduced in the late 1960s mounted on rosettes and have typical temperature and salinity accuracies of ±0.001°C and ±0.003, respectively. Finally, the Argo float program started in the early 2000s and CTD mounted on these floats are less accurate than those used on ships, with accuracies of ±0.002°C for temperature and ±0.01 for salinity, as they are not routinely calibrated (http://www.argo.ucsd.edu/Data_FAQ.html#accurate). Observational analyses at the TGB are limited to springtime observations because spring months (April, May and June) are the best sampled, containing 61% of all data, and because observations are sparse in other months, particularly before 1950. By limiting our analysis to a single well-sampled season, we avoid aliasing seasonal variability in our multidecadal time series. First, time series of isopycnal depths are obtained by cubic interpolation of a specific density using hydrographic vertical profiles. Second, we construct a spatially-varying springtime isopycnal depth by averaging over all observations in 0.5^o x 0.5^o

sub-domains of the TGB region. Third, we calculate isopycnal depth anomalies by subtracting the appropriate climatological mean from every observation within these subdomains. These anomalies are then averaged in overlapping 3-year windows to arrive at the black dots in Figure 3a and 3b. This procedure for calculating anomalies helps minimize the possibility for mistakenly interpreting variability in the location in which the observations were collected in the larger box as a change in properties at the TGB. Finally, a linear least squares regression is performed to find the temporal trend over the time series of anomalies. The resulting observational time series are compared with climate model output by computing isopycnal depth differences between *warming* and *pre-industrial control* scenarios averaged over the TGB and over each model year.

For all the analyses, density is derived from hydrographic data using the equation of state EOS-80 [32] because it is available in the software (NOAA/PMEL Ferret) that is amenable to analysis of large model output. Although EOS-80 has been superseded by the International Thermodynamic Equation Of Seawater-2010 (TEOS-10), the two algorithms return near identical density values in our region of interest. We have quantified these differences in terms of isopycnal depth anomaly time series. The root mean square difference between time series using TEOS-10 and EOS-80 is 1.9 m for $\sigma_\theta = 27.25\,\mathrm{kg\,m^{-3}}$ and 2.8 m for $\sigma_1 = 32.3\,\mathrm{kg\,m^{-3}}$, that is, much smaller than the standard error (shaded areas in Fig.3). Additionally, differences in isopycnal deepening trends between 1920 and 2010 are about 0.01 m, which is also much smaller than 95% confidence intervals, which are ± 0.2 m for $\sigma_\theta = 27.25\,\mathrm{kg\,m^{-3}}$ and ± 0.35 m for $\sigma_1 = 32.3\,\mathrm{kg\,m^{-3}}$.

Climate model. The GFDL climate model CM2.6 is a high-resolution coupled atmosphere-ocean-ice global model that includes a reduced-complexity ocean biogeochemical model [9]. The ocean

component (MOM5) has a spatial resolution of $1/10^{\circ}$, and 50 vertical levels, and the biogeochemical model (miniBLING [33]) consists of three prognostic tracers, dissolved inorganic carbon, phosphate, and oxygen. Human-induced biogeochemical inputs, such as nutrient loading, are not implemented.

The fully coupled model was spun-up for 72 years with atmospheric CO_2 fixed at a pre-industrial concentration (286 ppm). After the spin-up phase, two different scenarios were integrated for an additional period of 80 years: a *pre-industrial control* scenario in which atmospheric CO_2 is held constant, and a *warming* scenario in which CO_2 is increased at an annual rate of 1% until doubled. After doubling, which occurs at model year 70, atmospheric CO_2 was held constant for 10 additional years. We analyzed the full 80 year period of both simulations. Numerical time series for any given property χ are constructed as $\chi(t) = \chi(t=0) + \Delta\chi(t)$, where $\chi(t=0)$ is the value at the pre-industrial initial time (year 1860), and $\Delta\chi$ is the difference between the *warming* case and the same model year of the *pre-industrial* control case. In this way, the influence of any model drift is minimized.

Modeled and observational time dimensions are related through atmospheric CO_2. The climate model is forced by a rapid increase in CO_2 that resembles the RCP6 scenario, following $\mathrm{CO_2^{MOD}}(t^*) = 286\, e^{0.01\, t^*}$, where $t^* \in [0, 80]$ is the model time. Historical and projected future CO_2 time series are approximated by a quadratic polynomial of the form $\mathrm{CO_2^{OBS}}(t) = 0.01005\,(t - 1860)^2 - 0.9605\,(t - 1860) + 309.3$ for $t > 1860$, being $\mathrm{CO_2^{OBS}} = 286$ at $t = 1860$. The modeled time dimension is therefore transformed by a factor r that fulfills $\mathrm{CO_2^{MOD}}(t^*) = \mathrm{CO_2^{OBS}}(rt^*)$ (Fig. S7). Our intention is to put the modeled time series on a time axis that roughly corresponds

to the historical CO_2 trajectory. We acknowledge that transforming the time axis in order to relate the idealized model following a convention of 1% per year increase in atmospheric CO_2 to the historical period when atmospheric CO_2 was increasing at a slower rate, does not account for other forced changes due to atmospheric aerosols, non-CO_2 greenhouse gases, and ozone.

Most model analyses are performed on isopycnal surfaces, rather than at fixed depths, to avoid conflating shifts in water mass characteristics with the heaving of isopycnals. We focus on $\sigma_\theta = 27.25\,\mathrm{kg\,m^{-3}}$, because its simulated depth is close to the observed depth range within the Laurentian Channel (Fig. S8) and it remains isolated from the surface throughout the region, hence avoiding influence from local air-sea exchange. For the Scotian Shelf, analyses are performed on the 150 m horizontal level, where most measurements are available.

Quasi-streamfunction and wind stress curl. The quasi-streamfunction Ψ is defined so that $F_X \equiv -\partial\Psi/\partial y$ and $F_Y \equiv \partial\Psi/\partial x$, where the zonal flow is $F_X = \int_{z_1}^{z_0} u\,dz$ while the meridional is $F_Y = \int_{z_1}^{z_0} v\,dz$, being (u, v) the horizontal velocity components. These flows are depth-integrated over the upper 1000 m since our interest lies in the upper ocean circulation. Hence the net vertical transport is nonzero, or in other words, the lateral flow is not fully divergence-free, and therefore we called it quasi-streamfunction. Flows are computed on-line in the model, saved every five days, and we solve for Ψ by cross-differentiation of F_X and F_Y definitions. Finally, we average Ψ over the last 20 model years. This definition of Ψ has units of volume Sverdrup ($1\ \mathrm{Sv} \equiv 10^6\ \mathrm{m^3\,s^{-1}}$).

The curl of the wind stress vector $\vec{\tau} = (\tau_x, \tau_y)$ is approximated using finite differences as $\nabla_h \times \vec{\tau} \simeq \Delta\tau_y/\Delta x - \Delta\tau_x/\Delta y$. In order to unveil the large-scale pattern over the North Atlantic

we take $\Delta x = \Delta y = 2^\circ$ since grid spacings smaller than this threshold obscure the basin scale distribution.

Data availability. Hydrographic data at Cabot Strait, the Laurentian Channel Mouth, and the central Scotian Shelf come from the CLIMATE database (http://www.bio-iob.gc.ca/science/data-donnees/base/data-donnees/climate-climat-en.php). Oxygen data at Cabot Strait is available from the BioChem database (http://www.dfo-mpo.gc.ca/science/data-donnees/biochem/index-eng.html) and at the central Scotian Shelf is upon request from Catherine E. Brennan (cebrennan.climate@gmail.com). Historical data at the Tail of the Grand Banks has been extracted from the public global database HydroBase3 website (http://www.whoi.edu/science/PO/hydrobase/php/index.php). The CM2.6-miniBLING model output is available upon request from J.P.D (john.dunne@noaa.gov). Bathymetric data comes from the 2-minute Gridded Global Relief Data (ETOPO2) v2, which is publicly available (https://www.ngdc.noaa.gov/mgg/global/etopo2.html).

31. Warren, B. A. Nansen-bottle stations at the Woods Hole Oceanographic Institution. *Deep-Sea Research Part I*, **55 (4)**, 379–395 (2008).

32. Millero, F. J., Chen C.-T., Bradshaw A., & Schleicher, K. A new high pressure equation of state for seawater. *Deep Sea Research Part A* **27 (3)**, 255–264 (1980).

33. Galbraith, E. D. *et al.* Complex functionality with minimal computation: Promise and pitfalls of reduced-tracer ocean biogeochemistry models. *Journal of Advances in Modeling Earth Systems* **7(4)**, 2012–2028 (2015).

34. Gatien, M. G. A study in the slope water region south of Halifax. *Journal of the Fisheries Research Board of Canada* **33** 2213–2217 (1976).

35. Bisagni, J.J., Gangopadhyay A. & Sanchez-Franks A. Secular change and inter-annual variability of the Gulf Stream position, 1993-2013, 70°-55°W. *Deep Sea Research Part I* **125(C)**, 1–10 (2017).

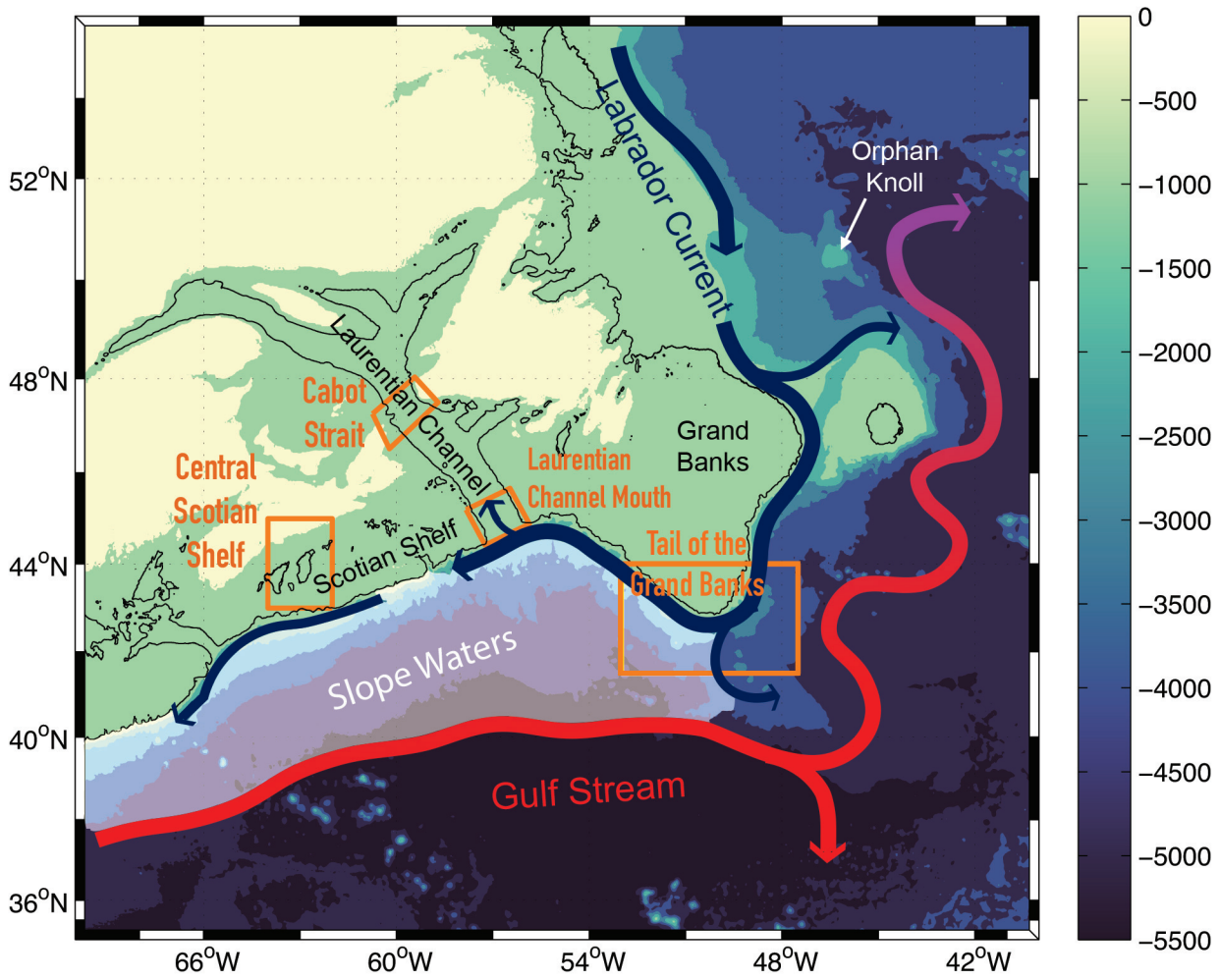

Figure 1: **Schematic of the large-scale circulation in the northwest Atlantic.** Labrador Current waters flow equatorward along the shelf break. At the Grand Banks, the Labrador Current must take a sharp right hand (westward) turn to flow along the shelf break and maintain a direct advective connection with the Slope Water region at the offshore edge of the Scotian Shelf and Laurentian Channel. Circulation on the slope mixes well-oxygenated Labrador Slope Water with oxygen-poor subtropical waters[34]. In turn, slope water masses (white shading) and circulation influence water properties on the continental shelf[28]. Bathymetry is indicated in color and the 200 m isobath as the solid contour. Circulation schematics follows geostrophic currents[35].

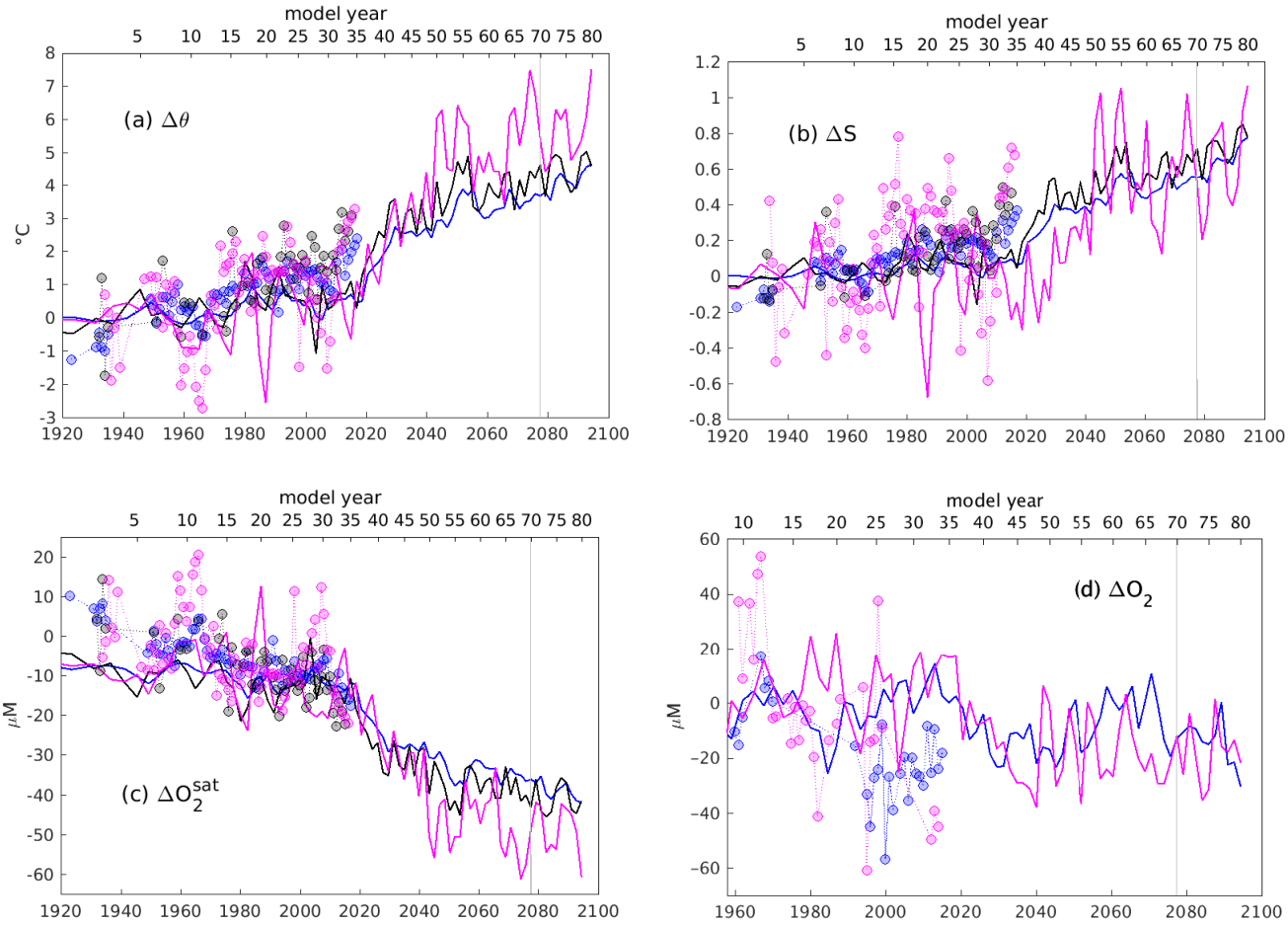

Figure 2: **Warming, salinity increase, and deoxygenation in the coastal northwest Atlantic**. Observational anomaly time series (dots) show the change in (a) potential temperature referenced to the surface (θ), (b) salinity (S), (c) oxygen saturation concentration (O_2^{sat}), and (d) oxygen (O_2) on the isopycnal $\sigma_\theta = 27.25\,\mathrm{kg\,m^{-3}}$ at Cabot Strait (blue, CS), the Laurentian Channel Mouth (black, LCM), and at 150m in the central Scotian Shelf (magenta, CSS). Anomalies are relative to a time average computed between 1920 and 1960 for θ, S, and O_2^{sat}. For O_2, the time average is between 1960 and 1970 at CS and between 1961 and 1999 at CSS. Standard error bars are shown in Figs. S1,S2. Time-series of change at the corresponding model locations (solid lines) are shown on a transformed time axis (upper axis) that roughly corresponds to the historical CO_2 trajectory (Methods). The vertical gray line in each panel denotes the year at which modeled atmospheric pCO_2 doubles relative to the pre-industrial value. Observed and modeled trends for each property at each location are provided in Figs. S1,S2. The depth evolution of isopycnal $\sigma_\theta = 27.25\,\mathrm{kg\,m^{-3}}$ at CS and the LCM is shown in Fig. S8.

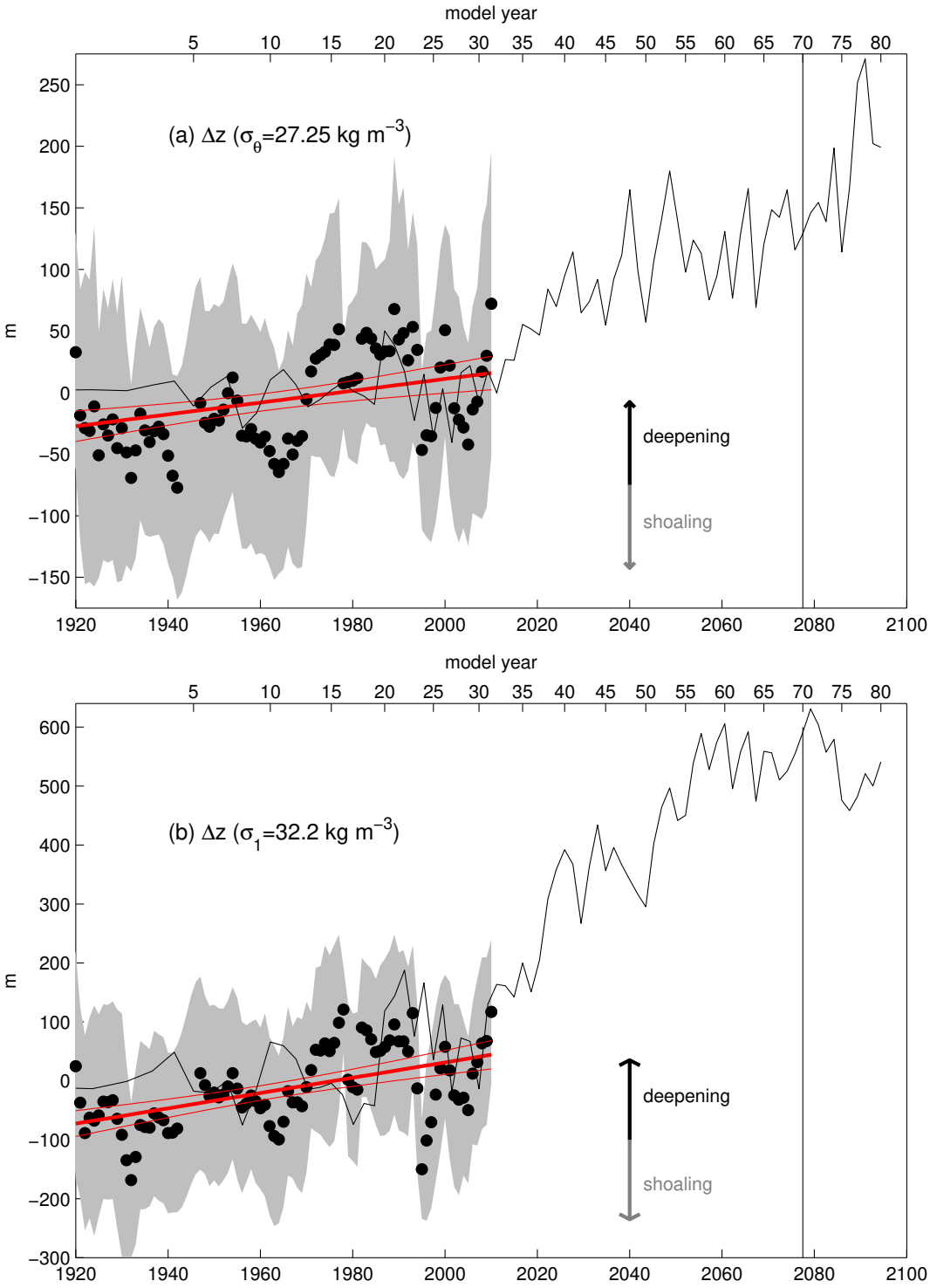

Figure 3: **Isopycnal depth anomalies at the Tail of the Grand Banks.** Depth anomalies of two isopycnals are plotted: (a) $\sigma_\theta = 27.25\,\mathrm{kg\,m^{-3}}$ and (b) $\sigma_1 = 32.2\,\mathrm{kg\,m^{-3}}$. Observations (dots) are 3-year averages from the region shown in Figure 1, calculated using springtime (April, May, June) data only, and are plotted with their standard deviation (shaded area). Also shown is a linear regression (thick red line) for each, with associated 95% confidence intervals (thin red lines). Model-simulated isopycnal depth anomalies, averaged over the same region for the warming simulation using the transformed time axis (see Figure 2 caption) are shown as solid black lines. A positive change in isopycnal depth corresponds to isopycnal deepening, interpreted as a gain of buoyant subtropical waters above the given isopycnal. See Methods for details.

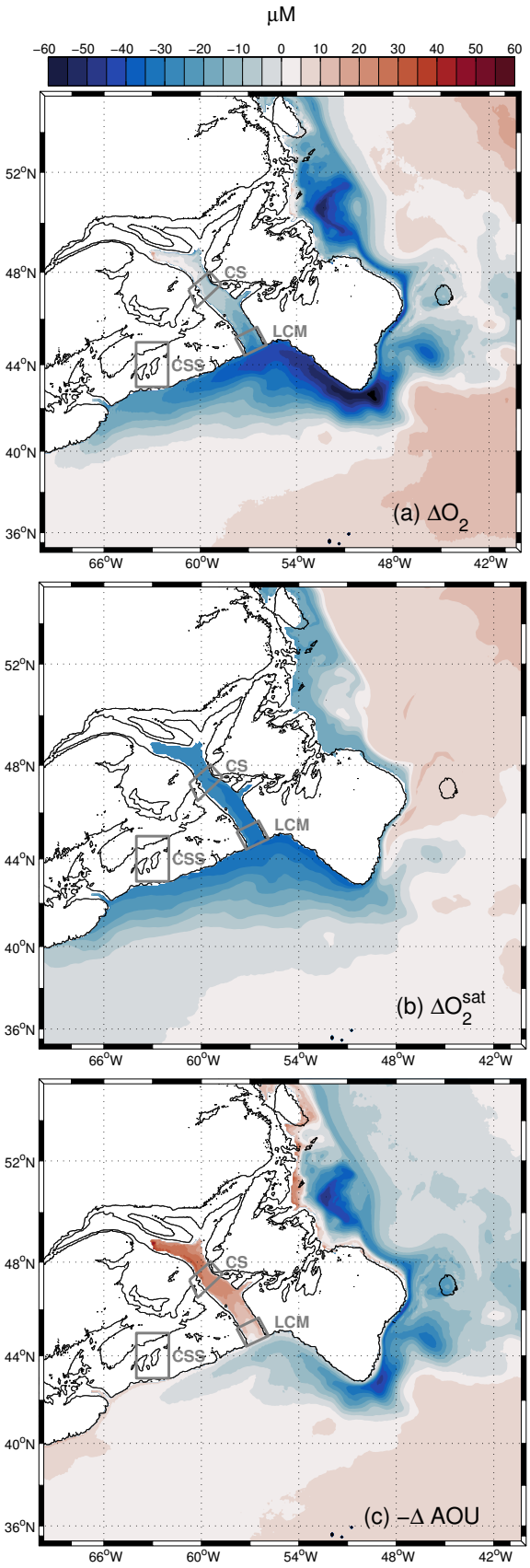

Figure 4: **Decomposition of the modeled oxygen decline with warming in the northwestern Atlantic.** Isopycnal maps on $\sigma_\theta = 27.25\,\mathrm{kg\,m^{-3}}$ of (a) the oxygen (O_2) change and its decomposition into changes of (b) oxygen saturation (O_2^{sat}) and (c) apparent oxygen utilization (AOU). Differences are computed relative to the *control* pre-industrial experiment and averaged over the last 20 model years. Locations where time-series are shown in Fig.2 are enclosed within gray polygons. Acronyms stand for the Laurentian Channel Mouth (LCM), Cabot Strait (CS), and the central Scotian Shelf (CSS).

Supplementary information supporting manuscript entitled "Rapid coastal deoxygenation due to ocean circulation shift in the NW Atlantic"

Mariona Claret*, Eric D. Galbraith, Jaime B. Palter, Daniele Bianchi, Katja Fennel, Denis Gilbert, & John P. Dunne

SUPPLEMENTARY FIGURES

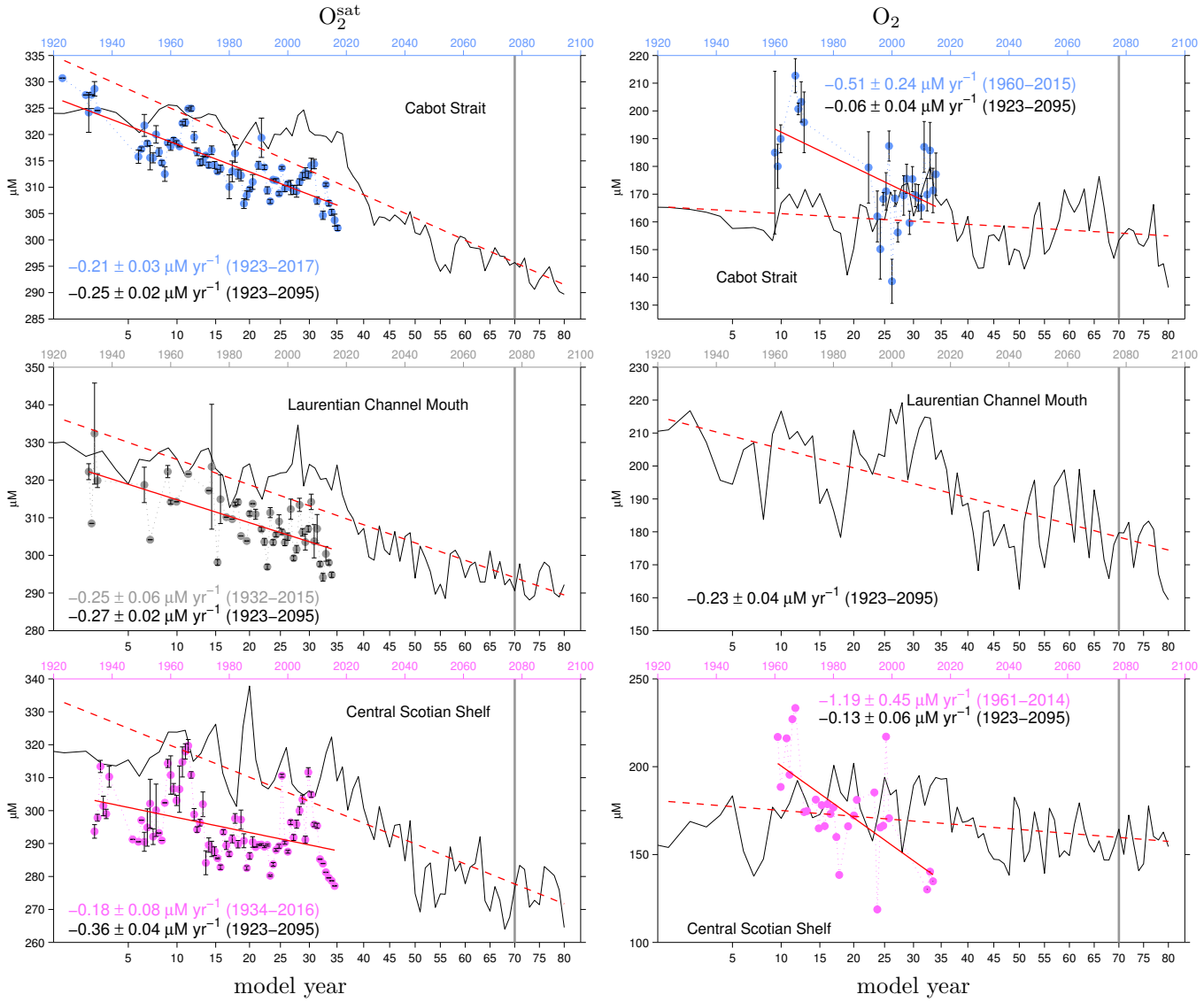

Figure S1. **Observational (dots) and modeled (solid black lines) deoxygenation time series in the Laurentian Channel and the Scotian Shelf.** Time series of oxygen saturation concentration (O_2^{sat}) and oxygen (O_2) on isopycnal $\sigma_\theta = 27.25\,\mathrm{kg\,m^{-3}}$ at Cabot Strait (blue) and at the Laurentian Channel Mouth (gray) and at 150 m depth in the central Scotian Shelf (magenta) plus/minus one standard error. For the O_2 time series at the central Scotian Shelf, only the standard deviation is known between 1961 and 1999 (24 μM, ref [6]), and between 2012 and 2014 the standard error is less than 0.2 μM given the high-frequency resolution of the benthic pod data. Observed and modeled trends are provided with 95% confidence intervals. These trends correspond to the red lines shown, solid lines for observations and dashed lines for model. Vertical solid line denotes the year at which modeled atmospheric pCO_2 is doubled relative to the pre-industrial 1860 historical value. See Methods for more data and analyses details.

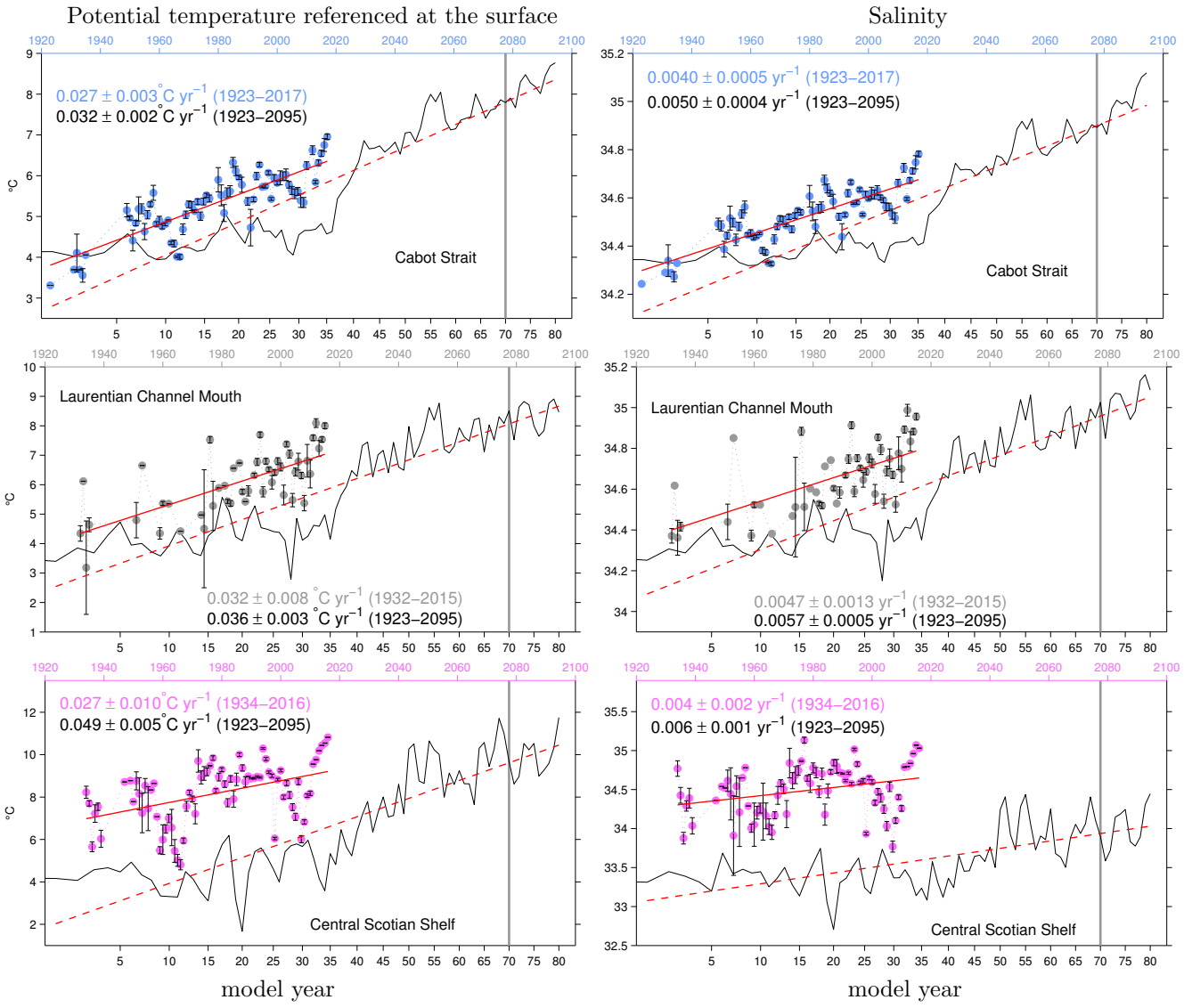

Figure S2. **Observational (dots) and modeled (solid black lines) hydrographic time series in the Laurentian Channel and the Scotian Shelf.** Same as Figure S1 for potential temperature and salinity.

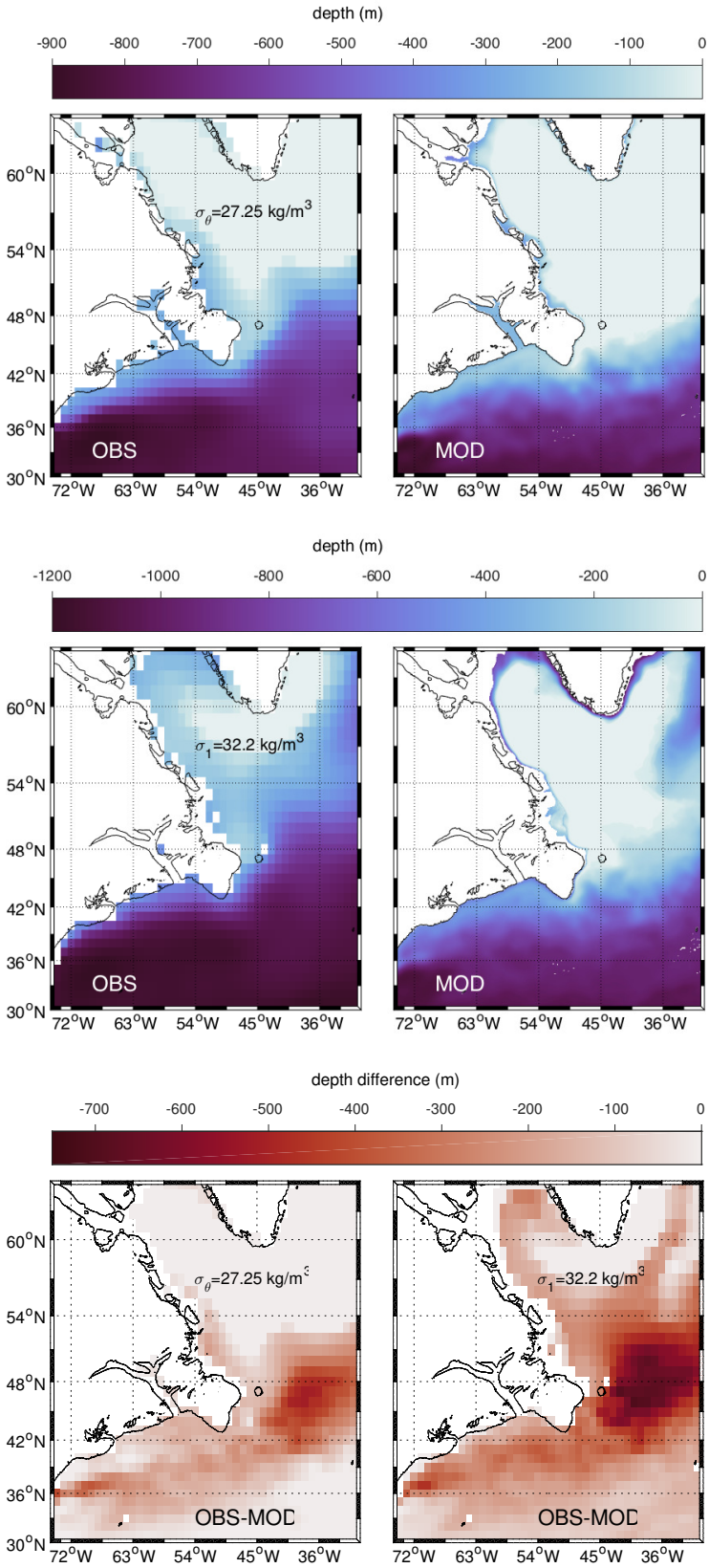

Figure S3. **Winter climatology for the northwest Atlantic of the depth of isopycnals $\sigma_\theta = 27.25\,\mathrm{kg\,m^{-3}}$ (top panels) and $\sigma_1 = 32.2\,\mathrm{kg\,m^{-3}}$ (middle panels) from observations (left) and model (right). Bottom panels show depth differences between observations and model for both isopycnals.** Observational data is from the World Ocean Atlas 2013 (https://www.nodc.noaa.gov/OC5/woa13/woa13data.html) and spans from 1955 to 2012, while modeled output is from the pre-industrial *control* scenario forced with atmospheric pCO_2 1860 historical value. The 200 m isobath is indicated for reference. Despite the notable differences between observations and model, in both cases isopycnals outcrop in the Labrador Sea and east of the Grand Banks for $\sigma_\theta = 27.25\,\mathrm{kg\,m^{-3}}$.

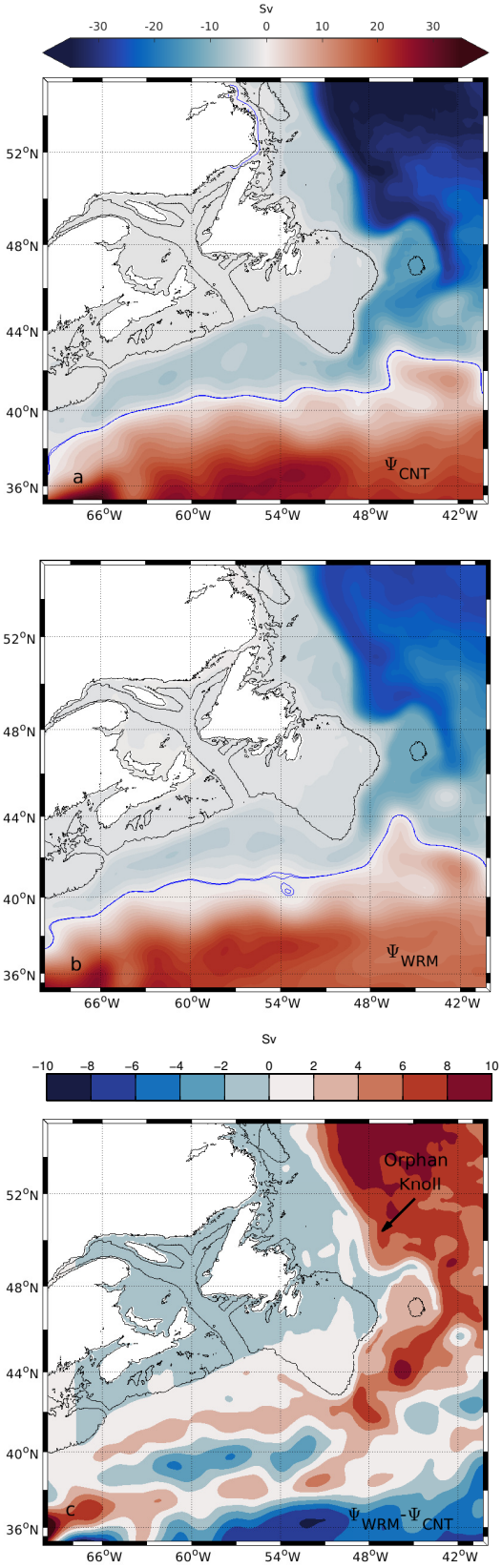

Figure S4. **Labrador Current weakening and impingement of the North Atlantic Current on the Tail of the Grand Banks in model.** Maps of the quasi-streamfunction Ψ, integrated over the upper 1000 m, averaged over the last twenty model years of (a) pre-industrial *control* (CNT) and (b) *warming* (WRM) modeled scenarios. The difference between both scenarios (c) is positive north of 40°N due to weakening of the Labrador Current and northward shift of the Gulf Stream. Between about 36°N and 40°N, the difference is negative due to a slowdown in the Gulf Stream. The 200 m isobath is indicated with a black line and the zero contour with a blue line for reference in (a) and (b). See Methods for details on the computation of Ψ.

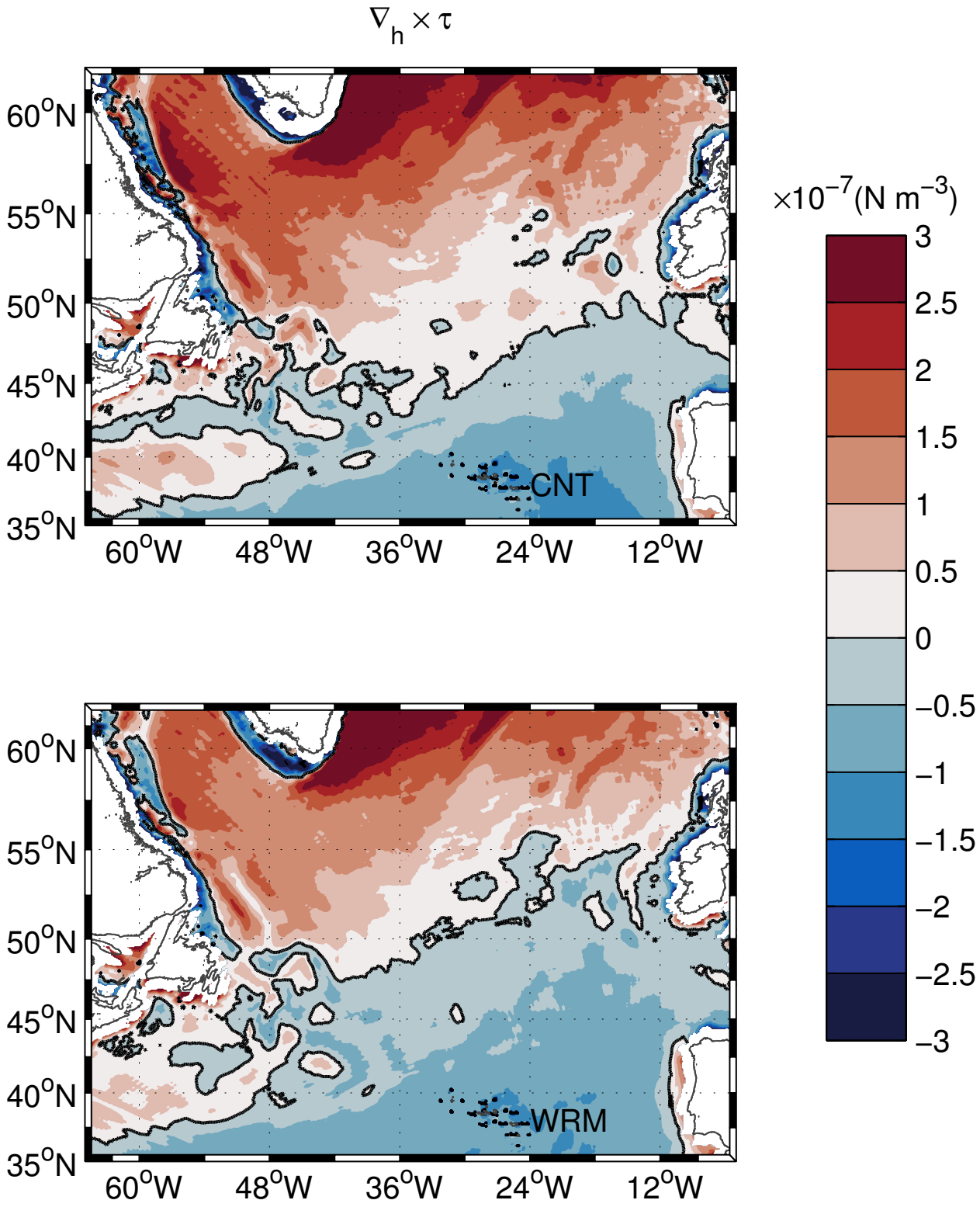

Figure S5. **Modeled weakening of the wind stress curl in the subpolar gyre and poleward shift of its zero line with warming in the North Atlantic**. Wind-stress curl is averaged over the last 20 model years of the pre-industrial *control* (CNT, top) and *warming* (WRM, bottom) scenarios. Zero contour is indicated with a solid black line. See Methods for details on the computation of the wind stress curl.

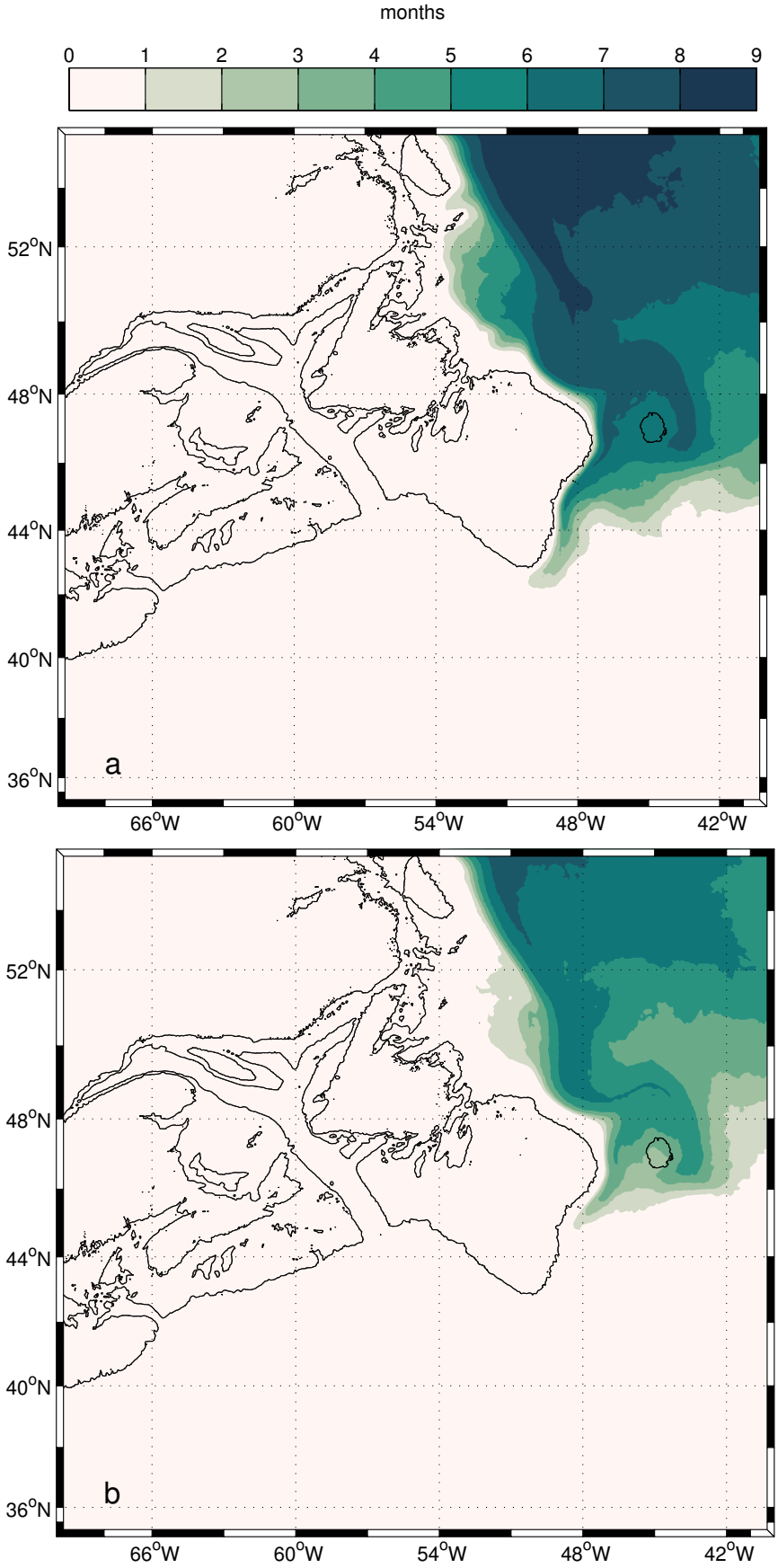

Figure S6. **Reduction of isopycnal outcropping.** Number of months isopycnal $\sigma_\theta = 27.25\,\mathrm{kg\,m^{-3}}$ outcrops averaged over the last twenty model years of (a) pre-industrial *control* and (b) *warming* experiments. The 200 m isobath is indicated with a black line for reference.

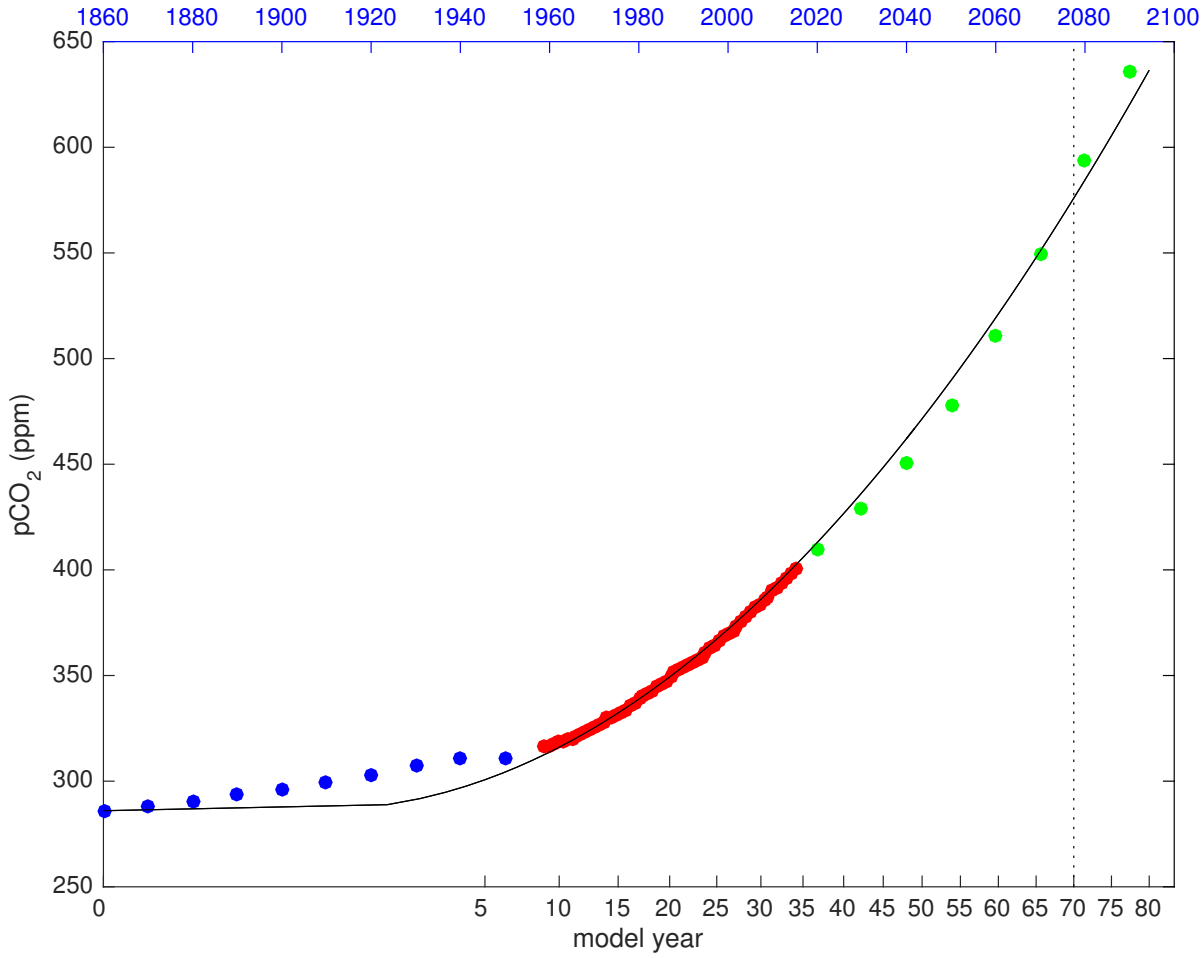

Figure S7. **Time dimension benchmark between CM2.6 model (line) and observations (dots).** Model and observations time dimensions are related through their atmospheric pCO_2. Specifically, the model time dimension is stretched using a polynomial quadratic function that fits to observational/modeled data. Blue dots correspond to CMIP5 recommended preindustrial conditions, red dots to the Mauna Loa Observatory in Hawaii (the so-called Keeling curve, www.esrl.noaa.gov/gmd/ccgg/trends), and green dots to future projections under the RCP6 scenario (https://tntcat.iiasa.ac.at/RcpDb).

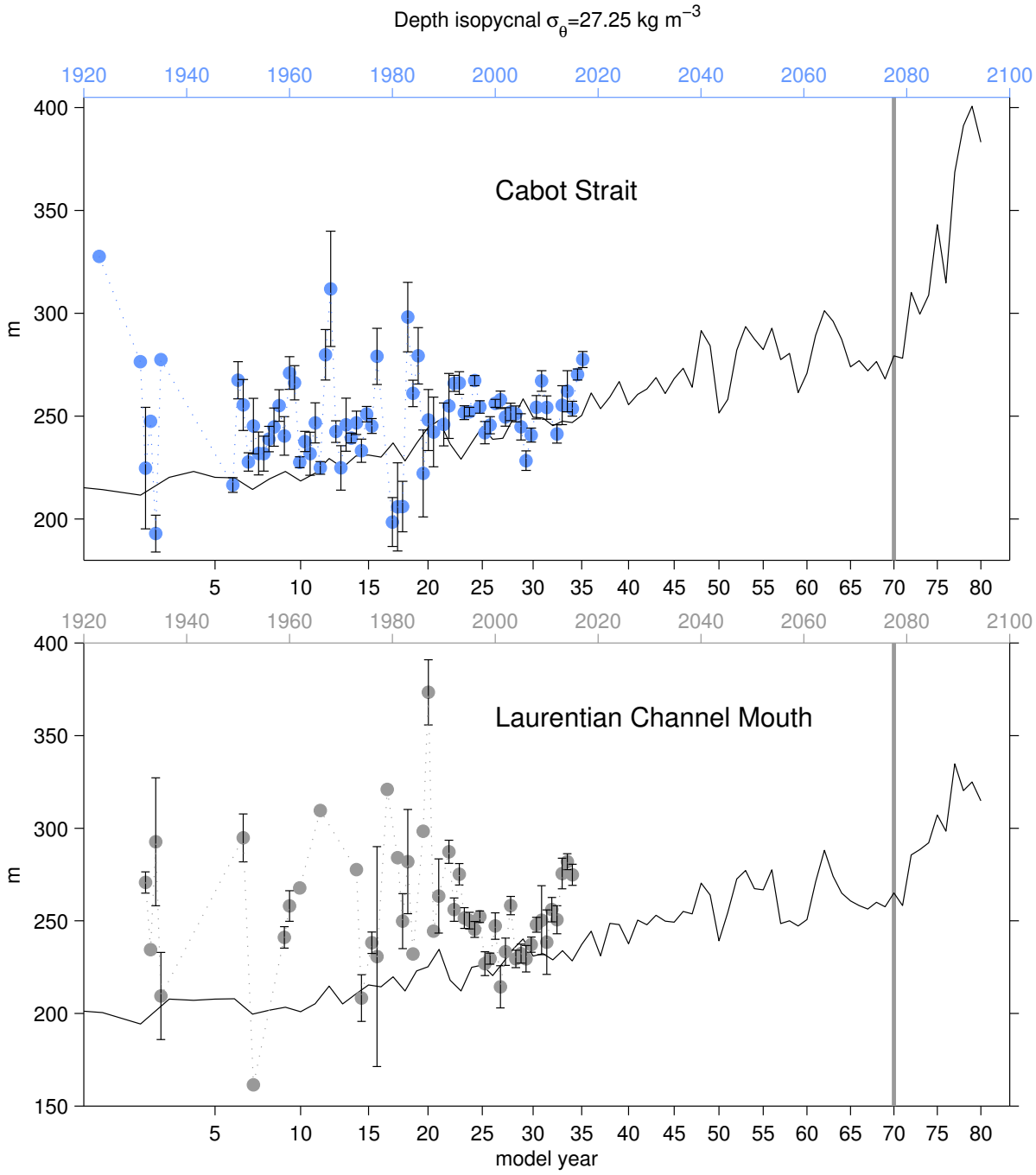

Figure S8. **Observational (dots) and modeled (solid lines) time series of the depth of isopycnal σ_θ = 27.25 kg m^{-3} within the Laurentian Channel.** Same as Figure S1 for the isopycnal depth at Cabot Strait and at the mouth of the Laurentian Channel.

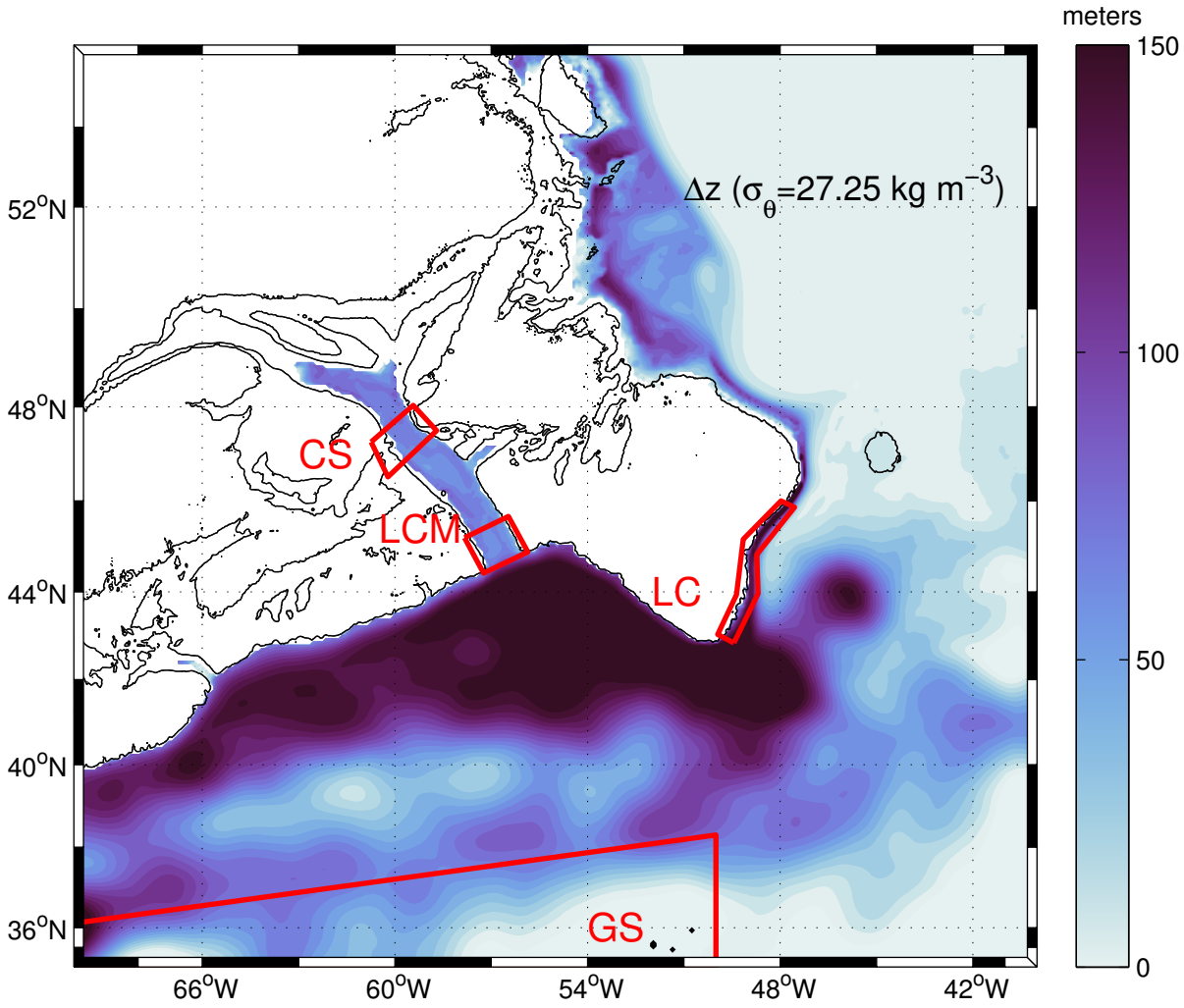

Figure S9. **Modeled deepening of isopycnal $\sigma_\theta = 27.25\,\mathrm{kg\,m^{-3}}$ with idealized warming.** Red boxes indicate regions within the Gulf of St. Lawrence (CS for Cabot Strait and LCM for the Laurentian Channel Mouth) and end member regions (GS for Gulf Stream and LC for Labrador Current). The 200 m isobath is included for reference.

SUPPLEMENTARY TEXT

Decomposition of oxygen changes using mixing model. One can gain further understanding of the simulated changes in oxygen (O_2) by considering the oxygen budget at any point as the sum of the *pre-formed* characteristics of source water masses advected into the region, weighted by their relative contributions, and Apparent Oxygen Utilization (AOU) accumulated along circulation pathways within the region. To this end, a two-end member mixing model (MIX) is constructed for the region with end members chosen to characterize the Gulf Stream (GS) water and the Labrador Current (LC) water immediately northeast of the Tail of the Grand Banks as defined in ref [1] (Fig. S9). The model is applied to an isopycnal surface and considers both oxygen saturation concentration $O_2^{\rm sat}$ and AOU to separate hydrographic effects on O_2 solubility from remineralization processes. Given that AOU is not a conservative tracer, we add a term ($AOU^{\rm path}$) equal to the total remineralization along the path of water mass transport (i.e. that not accounted for by the end member mixing) to obtain

$$\begin{aligned} \mathrm{O_2} &= f\mathrm{O_2^{LC}} + (1-f)\mathrm{O_2^{GS}} - \mathrm{AOU^{path}} \\ &= \underbrace{f\,\mathrm{O_2^{sat,LC}} + (1-f)\,\mathrm{O_2^{sat,GS}}}_{\mathrm{O_2^{sat,MIX}}} \underbrace{-f\,\mathrm{AOU^{LC}} - (1-f)\,\mathrm{AOU^{GS}}}_{-\mathrm{AOU^{MIX}}} - \mathrm{AOU^{path}}, \end{aligned} \tag{1}$$

where f is the fraction of the LC water mass and $1-f$ is that of the GS. These water mass fractions are obtained by solving the following linear system of equations, based on two-end member mixing models for potential temperature referenced at the surface (θ) and salinity (S),

$$\theta = f\,\theta^{\rm LC} + (1-f)\,\theta^{\rm GS}$$

$$\mathrm{S} = f\,\mathrm{S^{LC}} + (1-f)\,\mathrm{S^{GS}},$$

using a least squares fit. End member properties averaged over the last two decades of the climate model are shown in Table S1. The AOU of end members is computed as the modeled difference between $O_2^{\rm sat}$ and O_2. The $AOU^{\rm path}$ is computed as the average of differences between the phosphate concentration (PO_4)

of one end member and that at the location where the mixing model is applied. Phosphate differences are calculated on isopycnals and weighted by the water mass fraction of the corresponding end member. This weighted-averaged phosphate difference is then multiplied by the oxygen to phosphate ratio O_2:P=-150, that is,

$$\mathrm{AOU}^{\mathrm{path}} = -150\left\{f(\mathrm{PO}_4^{\mathrm{LC}} - \mathrm{PO}_4) + (1-f)(\mathrm{PO}_4^{\mathrm{GS}} - \mathrm{PO}_4)\right\}. \tag{2}$$

In order to examine the downstream effects of changes in the LC fraction, we take the Laurentian Channel Mouth site as an example and use averaged values over the last twenty model years. Here, as shown in Table S2, the Labrador Current water mass fraction is halved, decreasing $\mathrm{O}_2^{\mathrm{sat,MIX}}$ and raising *pre-formed* AOU ($\mathrm{AOU}^{\mathrm{MIX}}$) for a total *pre-formed* oxygen decrease of 54 $\mu\mathrm{mol\,kg}^{-1}$. In the model, but not in nature (see Fig. 2), there is a large decline in the AOU accumulated along the circulation pathway ($\mathrm{AOU}^{\mathrm{path}}$) which counteracts more than half of the end-member- and mixing-driven O_2 decrease. Since the isopycnal does not outcrop west of the Grand Banks (Fig. S6), the decrease of AOU must reflect a decrease in the cumulative consumption of oxygen. The decreased oxygen consumption in the model could be attributed to a reduced residence time of waters in the region and/or a reduced rate of oxygen consumption, the latter of which arises from decreased export production as the region stratifies, and is exacerbated as a reduced fraction of the total remineralization occurs on this deepening isopycnal surface [2] (Fig. S9).

The results shown in Table S1 also reveal a significant decrease in the oxygen content of the Labrador Current end member in the *warming* case scenario, with saturation oxygen decreasing by 13 $\mu\mathrm{mol\,kg}^{-1}$ and AOU increasing by 15 $\mu\mathrm{mol\,kg}^{-1}$, while the Gulf Stream end member remains more stable given that the isopycnal does not outcrop at this location (the shallowest depth is reached in the *control* case at 540 m), therefore it is not directly influenced by atmospheric forcing. The decrease in $\mathrm{O}_2^{\mathrm{sat}}$ in the LC end member is due to surface warming and an enrichment of subtropical water in the region as the LC retreats, while the AOU increase can be attributed to a reduction of the exposure of the isopycnal at the surface upstream

of the Grand Banks, resulting from enhanced stratification (Fig. S6), which cuts off the oxygen supply to the isopycnal at its source. To quantify the relevance of LC end member oxygen changes with warming to deoxygenation at the Laurentian Channel Mouth, we next quantify its contribution and compare it with that due to changes in the proportion of water masses.

The oxygen change can be decomposed in terms of end member changes as follows. Defining the change between warming (WRM) and control (CNT) cases as $\Delta \mathrm{O}_2 = \mathrm{O}_2(\mathrm{WRM}) - \mathrm{O}_2(\mathrm{CNT})$ and considering the oxygen decomposition into $\mathrm{O}_2^{\mathrm{sat,MIX}}$, $\mathrm{AOU}^{\mathrm{MIX}}$, and $\mathrm{AOU}^{\mathrm{path}}$, applying the finite difference operator Δ to equation (1) gives

$$\Delta \mathrm{O}_2 = \Delta \mathrm{O}_2^{\mathrm{sat,MIX}} - \Delta \mathrm{AOU}^{\mathrm{MIX}} - \Delta \mathrm{AOU}^{\mathrm{path}}. \tag{3}$$

After applying the product rule of forward differences, changes in $\mathrm{O}_2^{\mathrm{sat,MIX}}$ and $\mathrm{AOU}^{\mathrm{MIX}}$ can be expressed as

$$\begin{aligned} \Delta \mathrm{O}_2^{\mathrm{sat,MIX}} &= \underbrace{\Delta f \left[\mathrm{O}_2^{\mathrm{sat,LC}}(\mathrm{CNT}) - \mathrm{O}_2^{\mathrm{sat,GS}}(\mathrm{CNT})\right]}_{\text{transport}} \\ &+ \underbrace{f(\mathrm{CNT}) \left[\Delta \mathrm{O}_2^{\mathrm{sat,LC}} - \Delta \mathrm{O}_2^{\mathrm{sat,GS}}\right] + \Delta \mathrm{O}_2^{\mathrm{sat,GS}}}_{\text{endmember}} \\ &+ \underbrace{\Delta f \left[\Delta \mathrm{O}_2^{\mathrm{sat,LC}} - \Delta \mathrm{O}_2^{\mathrm{sat,GS}}\right]}_{\text{nonlinear}}, \end{aligned} \tag{4}$$

$$\begin{aligned} \Delta \mathrm{AOU}^{\mathrm{MIX}} &= \underbrace{\Delta f \left[\mathrm{AOU}^{\mathrm{LC}}(\mathrm{CNT}) - \mathrm{AOU}^{\mathrm{GS}}(\mathrm{CNT})\right]}_{\text{transport}} \\ &+ \underbrace{f(\mathrm{CNT}) \left[\Delta \mathrm{AOU}^{\mathrm{LC}} - \Delta \mathrm{AOU}^{\mathrm{GS}}\right] + \Delta \mathrm{AOU}^{\mathrm{GS}}}_{\text{endmember}} \\ &+ \underbrace{\Delta f \left[\Delta \mathrm{AOU}^{\mathrm{LC}} - \Delta \mathrm{AOU}^{\mathrm{GS}}\right]}_{\text{nonlinear}}. \end{aligned} \tag{5}$$

In the above equations, terms involving changes in the fraction of water masses Δf are driven by changes in transport and terms involving changes of the end members are driven by changes in ventilation for AOU and warming for $\mathrm{O}_2^{\mathrm{sat}}$.

The above decomposition of O_2 changes works well in the Laurentian Channel as shown in Table

S3. The sum of terms in equations (4,5) is in agreement with changes directly computed using the two-end member mixing model (Tables S1, S2). The largest decline in O_2^{sat} and AOU is explained by the transport term, representing a fraction of about 2/3 of the terms contributing to O_2 loss, due to a reduction of the Labrador Current Water transport west of the Tail of the Grand Banks. The remaining fraction of the O_2 decline is explained by changes in the LC end member (endmember and nonlinear terms) associated with warming (decline in $O_2^{sat,LC}$) and a reduction in ventilation (increase in AOU^{LC}). Therefore, property changes in the subpolar end member are non-neglible and should be taken into account when constructing O_2 mixing models in this region.

1. Gilbert, D., Sundby, B., Gobeil, C., Mucci, A. & Tremblay, G.-H. A seventy-two-year record of diminishing deep-water oxygen in the St. Lawrence estuary: The northwest Atlantic connection. *Limnology and Oceanography* **50**, 1654–1666 (2005).

2. Deutsch, C., Brix, H., Ito T., Frenzel H. & Thompson L. Climate-Forced Variability of Ocean Hypoxia *Science* **333**, 336–339 (2011).

SUPPLEMENTARY TABLES

	End member compositions							
	Labrador Current				Gulf Stream			
	θ^{LC}	S^{LC}	$\mathrm{O}_2^{\mathrm{sat,LC}}$	$-\mathrm{AOU}^{\mathrm{LC}}$	θ^{GS}	S^{GS}	$\mathrm{O}_2^{\mathrm{sat,GS}}$	$-\mathrm{AOU}^{\mathrm{GS}}$
CNT	2.6	34.19	328	-41	10	35.39	274	-80
WRM	4.2	34.35	315	-56	9.9	35.37	275	-75
Δ	1.6	0.16	-13	-15	-0.1	-0.02	1	5

Table S1. Changes at the Labrador Current (LC) and Gulf Stream (GS) end member locations of potential temperature (θ in °C), salinity (S), saturation oxygen concentrations ($\mathrm{O}_2^{\mathrm{sat}}$) and Apparent Oxygen Utilization (AOU), both in $\mu\mathrm{mol\,kg}^{-1}$, are shown. All values are averaged over the last twenty years of the pre-industrial *control* (CTR) and *warming* (WRM) climate model scenarios, on the $\sigma_\theta = 27.25\,\mathrm{kg\,m}^{-3}$ isopycnal or at the surface where isopycnal outcrops. Changes (Δ) are computed relative to the pre-industrial *control*, that is, Δ=WRM-CTR for any given property.

	Laurentian Channel Mouth						
	f^{LC}	O_2	O_2^{sat}	$-AOU$	$O_2^{sat,MIX}$	$-AOU^{MIX}$	$-AOU^{path}$
CNT	0.86	219	319	-100	320	-46	-57
WRM	0.34	197	287	-90	288	-68	-18
Δ	-0.52	-22	-32	10	-32	-22	39

Table S2. As in Table S1 but at the Laurentian Channel Mouth (LCM) location. Also shown, are the fraction of Labrador Current water (f^{LC}) and the decomposition of oxygen concentrations following $O_2 = O_2^{sat} - AOU = O_2^{sat,MIX} - AOU^{MIX} - AOU^{path}$, where $O_2^{sat,MIX}$ and AOU^{MIX} are the mixing product of the *pre-formed* end member characteristics, weighted by their proportional contributions as given by f^{LC}. The property AOU^{path} is the AOU accumulated along the pathway from the end members to the LCM site. This simple two end member model works particularly well in this region for O_2^{sat} as shown by the agreement between changes in $O_2^{sat,MIX}$ and changes in the actual O_2^{sat}. Oxygen units are $\mu mol\,kg^{-1}$.

	transport	endmember	nonlinear	SUM
$\Delta O_2^{sat,MIX}$	-28	-11	7	**-32**
$-\Delta AOU^{MIX}$	-20	-12	10	**-22**

Table S3. Changes in O_2^{sat} and AOU along isopycnal $\sigma_\theta = 27.25\,kg\,m^{-3}$ decomposed into changes driven by a change in water mass fraction (transport), a change in end member properties (end member), and both (nonlinear). The sum of the three three terms (SUM) is in close agreement with changes directly quantified from the mixing model (Table S2). Units are $\mu mol\,kg^{-1}$. All values are averaged over the last twenty years of the pre-industrial *control* and *warming* climate model scenarios.

SUPPLEMENTARY VIDEO

Video S1: Time evolution of simulated O_2 in the northwest Atlantic on isopycnal $\sigma_\theta = 27.25\,\mathrm{kg\,m^{-3}}$ over the last twenty model years (from 181 to 200) for pre-industrial *control* (LEFT) and *warming* (1% annual pCO_2 increase until doubled, RIGHT) scenarios. Climate model horizontal resolution is $1/10^\circ$ and the time period between movie frames is five days. The movie shows that the oxygen supply to slope waters (white shading in Fig. 1) and the Laurentian Channel decreases significantly under warming due to a reduction in transport of ventilated Labrador Current waters west of the Tail of the Grand Banks. Isopycnal outcrop is shown in white.